Computational Modeling of Tissue Engineering Scaffolds as Delivery Devices for Mechanical and Mechanically Modulated Signals

Min Jae Song, David Dean and Melissa L. Knothe Tate

Abstract In this chapter, we outline the use of computational modeling and novel experimental methods to develop tissue engineering scaffolds as delivery devices for exogenous and endogenous cues, including biochemical and mechanical signals, to drive the fate of mesenchymal stem cells (MSCs) seeded within. Tissue regeneration in mature organisms recapitulates de novo tissue generation during organismal development. This gave us the impetus to develop tissue engineering scaffolds that deliver mechanical and chemical cues intrinsic to the environment of cells during mesenchymal condensation, which marks the initiation of skeletogenesis during development. Cell seeding density and mode of achieving density (protocol) have been shown to effect dilatational (volume changing) stresses on stem cells and deviatoric (shape changing) stresses on their nuclei. Shear flow provides a practical means to deliver mechanical forces within scaffolds, resulting in both dilatational and deviatoric stresses on cell surfaces. Both spatiotemporal mechanical cue delivery and mechanically modulated biochemical gradients can be further honed through optimization of scaffold geometry and mechanical properties. We use computational fluid dynamics (CFD) coupled with finite element analysis (FEA) modeling to predict flow regimes within the scaffolds and optimize flow rates to simulate seeded cells. This chapter outlines to major advantages of using computational modeling to design and optimize tissue engineering scaffold geometry, material behavior, and tissue ingrowth over time.

M. J. Song · D. Dean · M. L. Knothe Tate (✉)
Case Western Reserve University, 10900 Euclid Avenue,
Cleveland, OH 44106, USA
e-mail: mkt4@case.edu

Stud Mechanobiol Tissue Eng Biomater (2013) 10: 127–143
DOI: 10.1007/8415_2012_138

Published Online: 7 June 2012

1 Introduction

During physiological activity, external loads in dynamic environments get transduced via the musculoskeletal system to the cells which build, maintain, and remodel musculoskeletal tissues. This loading of poroelastic, viscoelastic, and hyperelastic fluid-imbibed solid elements and complex fluids transduces dilatational mechanical stresses, which induce volume without shape changes, and deviatoric mechanical stresses, which induces shape without volume changes. In this way, ground forces transduced via the muscles, ligaments, tendons and bones are experienced as stresses at the tissue length scale (e.g., cortical or trabecular bone, tendon) and cellular length scale (e.g., osteocytes in the pericellular lacunocanalicular system, or tenocytes), respectively [6, 24, 33]. (Fig. 1) Osteocytes and tenocytes have a crucial role in sensing these mechanical signals through a putative feedback system that enables maintenance and remodeling of bone, respectively tendon, tissue structure and function in dynamic environments [9, 23].

Taking into account these typical examples of mechanoadaptation as a means to maintain structure–function relationships in tissues exposed to spatiotemporally dynamic mechanobiological environments, new strategies for engineering and manufacture of replacement tissues are incorporating biomimicry approaches to harness nature's smart biomaterial paradigms. The design and engineering of tissue engineering scaffolds has entered a new era, where such scaffolds are considered as much as delivery devices as structural and functional tissue replacements [2, 26]. To harness nature's paradigms, we aim to drive structure–function relationships at the tissue and organ length scales by delivering appropriate mechanical and chemical cues to cells. One approach to optimize scaffolds as delivery devices is to use predictive computational modeling as a powerful tool that "…help[s] us to prioritize which variables exert dominant effects on system behavior and thus which experiments are key to test predictions. [As such] predictive computational model[s] allow for the study of [tissue's smart, multiscale properties] without the imperative to carry out thousands of experiments," as summed up in a recent publication [25]. In this chapter, we review computational modeling of tissue engineering scaffolds as delivery devices for mechanical and mechanically modulated (biological and chemical) signals.

Computational models can predict and simulate the role of mechanical forces in cell differentiation, motility, adhesion, proliferation, and secretion of extracellular matrix proteins within tissue engineering scaffold environments. The computational method even helps to unravel the most enigmatic problems whose solutions are stymied by experimental or technological limitations. For example, experimental mechanical testing of the femur can elucidate boundary stresses and strains; in contrast, computational models can predict intrinsic mechanical loading distributions of the structure after experimental validation. With a given tissue engineering scaffold geometry, computational models can be used to control and optimize parameters to deliver mechanical stimuli to cells seeded within, in order to maximize the probability of achieving the targeted tissue manufacture and integration. (Fig. 2) [2].

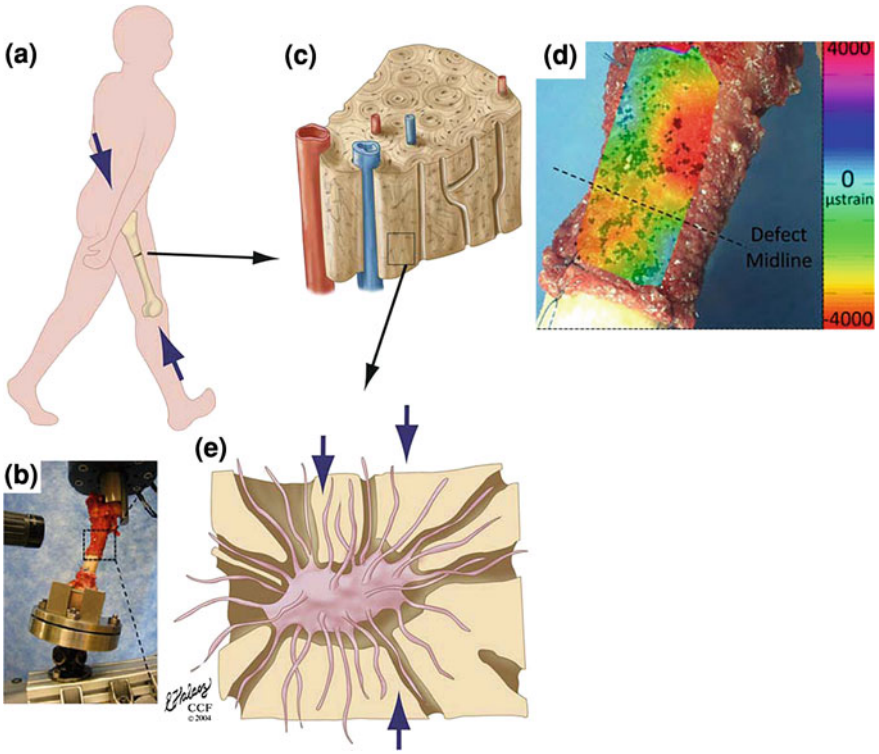

Fig. 1 Physiological loading of a patient or subject in a dynamic environment, from the organ length scale (**a**) in vivo and (**b**) ex vivo, tissue length scale (**c**) for cortical bone within the periosteum (**d**), and cellular length scale (pericellular, lacunocanalicular fluid space, (**e**) *Adapted from* [24]. **b** Ex vivo experimental set up for compressive loading of the femur to mimic stance shift in the first 2 weeks after one stage bone transport surgery. **d** Example of high-definition optical strain mapping for periosteum surrounding a critical sized defect which is exposed ex vivo to mechanical loads mimicking stance shift after surgery (**b**). *Adapted from* [24, 33], used with permission

CFD models allow for study of flow induced forces at multiple length and time scales. Given the importance of the fluid environment for all cells of the body, this chapter emphasizes aspects of CFD for engineering and manufacture of tissues, using bone and treatment of bone defects as a case study.

2 Tissue Engineering Scaffold for Treatment of Critical Sized Bone Defects

Critical sized defects (CSDs) in bone are defined as the smallest defects that cannot heal spontaneously during the lifetime of a patient or study subject. Such critical sized defects are commonly caused after trauma, neurosurgical interventions, and reconstructive surgery of congenital abnormality, cancer, and infections. The

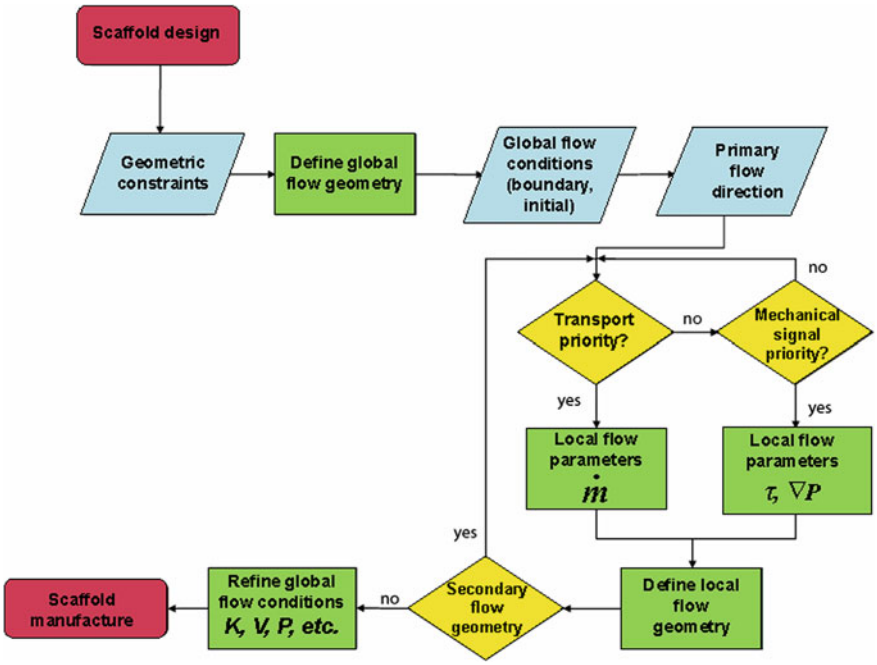

Fig. 2 Flow chart for design and optimization of tissue engineering scaffolds using CFD as a predictive tool. CFD multiphysics methods demonstrate chemical transport and delivery of mechanical signals within a given tissue engineering scaffold geometry, such as that shown in Fig. 3 where the primary flow direction is axial (along the length of the cylinder) and the secondary flow direction is orthogonal (transverse, defined by secondary flow geometry). *Adapted from* [2], used with permission. Please refer to online version of chapter for color version of the figure

current standard treatment option for such defects involves bone grafting, where graft is obtained from the patient himself (autograft), a bone bank (allograft), a graft substitute, or a structural implant or filler such as titanium or poly-methylmethacrylate (PMMA). Autografts are the gold standard treatment for CSDs due to their lack of immunogenicity; immune rejection is a critical complication associated with use of allograft. One complication associated with the use of autograft for CSDs, particularly of the cranium, is poor vascularization, which results in the need for reoperations and/or the removal of the implant [19]. In addition, packing of CSD with morcellized bone graft has been shown recently to retard the ingression of MSCs from the periosteum, when it is left in situ around the defect zone [29]. Furthermore, success of the surgery depends highly on both the size of the defect and the quality of its surrounding tissue [28]. Even with a sufficiently small defect that is surrounded by a healthy tissue bed, autografting *per se* is associated with risks including donor site morbidity and additional pains [19, 38].

Over the past several decades, tissue engineering has been developed as an alternative to tissue transplantation. For CSDs of long bone, a new surgical technique referred to as the one-stage bone transport procedure has been developed

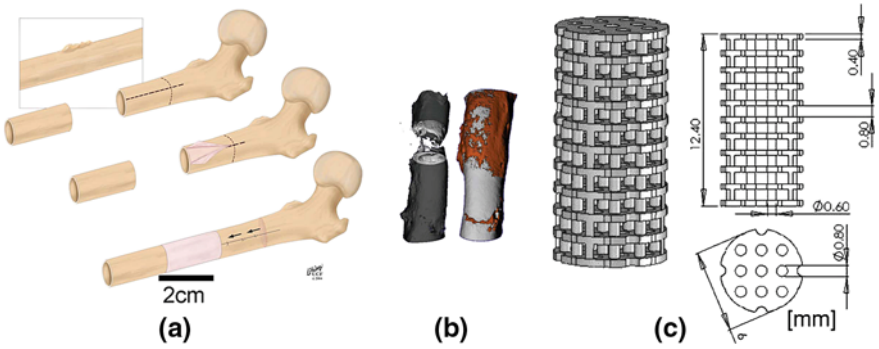

Fig. 3 Schematic of the one-stage bone-transport surgical procedure applied to the femur **a** and **b** three-dimensional (3D) micro-computed tomograph reconstruction of the critical sized defect control (unhealed after 16 weeks) and the defect surrounded by healthy periosteum in situ (healed completely after 16 weeks) [28], used with permission. **c** Computer Aided Design (CAD) drawings of 3D scaffold designs for treatment of CSD in the cranium [13, 18], adapted from [13] and used with permission . Please refer to online version of chapter for color version of the figure

recently (Fig. 3a, b) [28]. The technique results in woven bone regeneration in CSD zone within 2 weeks of surgery. Recent studies using a periosteum replacement implant *cum* delivery device have shown that incorporation of periosteal factors, including periosteum derived multipotent cells and periosteal strips without patent blood supply, around the defect zone can improve defect infilling compared to that observed with baseline controls [26]. For cranial CSDs, polymer scaffolds have been designed, some of which also incorporate MSCs (Fig. 3c) [13, 18]. This scaffold consists of polypropylene fumarate (PPF) mixed with a photoinitiator, which can be cross-linked by exposing it to a concentrated flood of UV light [13]. MSCs are seeded into the scaffold before implantation of this scaffold into cranial CSD zone. Broad interdisciplinary studies are in progress to elucidate mechanisms of tissue building, incorporating fundamentals of computational and experimental mechanics, polymer science, rapid prototyping, biochemistry, and stem cell mechanobiology [39, 41].

3 Mechanical Characteristics of Embryonic Stem Cells

Biophysical and biochemical cues define the local environment of the cell and play a key role in determining cell behavior including migration, proliferation, and differentiation; cumulatively, these cell behaviors result in de novo generation of tissue or bottom up tissue engineering. During embryonic development, cells respond to biophysical and biochemical signals to form the template of the complete organism. Defining the tissue template specifications to mimic the environment of the condensed mesenchyme (Fig. 4) during development allows

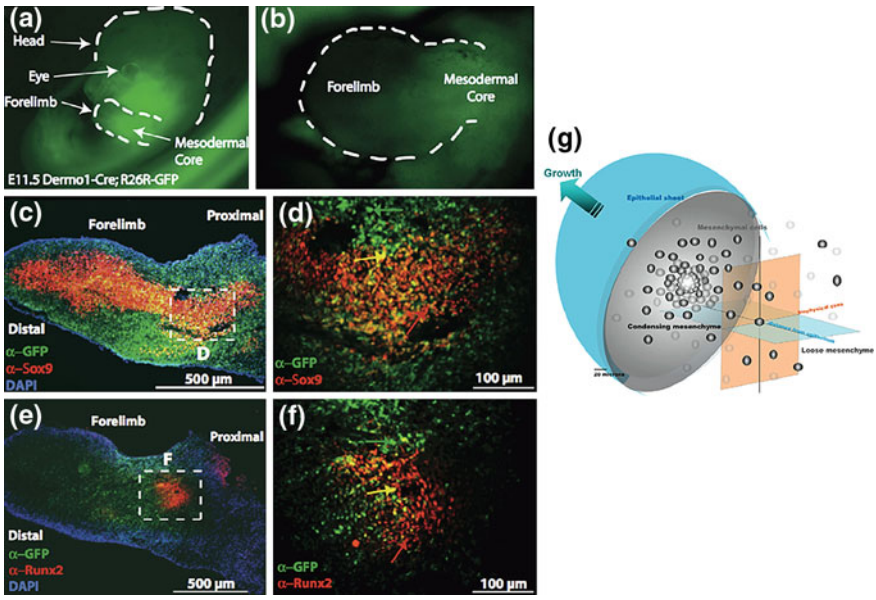

Fig. 4 Key extrinsic factors and their role in mesenchymal condensation, the first step of skeletogenesis. (**a**, **b**) The embryonic murine limbud is shown at E11.5, where the mesenchyme is bulbous in shape. Although possessing the same genetic code, lineage commitment by each cell is highly dependent on spatiotemporal signals including deviatoric and dilatational stress states as well as the biochemical *milieu*. For example, the expression of Sox9, a genetic marker of chondrogenesis (**c**, enlarged in **d**) is spatially distinct from that of Runx2, a genetic marker of osteogenesis (**e**, enlarged in **f**). *Adapted from* [27], used with permission

for exploitation of tissue scaffolds as delivery devices for exogenous and endogenous cues, including biochemical and mechanical signals, to drive the fate of MSC seeded within [27].

Recent studies demonstrate the promise of delivering spatiotemporally controlled mechanical cues to guide stem cell proliferation patterns [2, 14, 25] and lineage commitment [2–5, 12, 24–26, 34, 35, 46], essentially harnessing nature's approach to engineering tissues. Moreover, embryonic MSC exhibit 1000-fold greater mechanosensitivity than terminally differentiated cells (Fig. 5) [2, 12, 34, 35, 46]. Already half a century ago, Pauwels postulated that dilatational stresses such as hydrostatic or normal stresses cause differentiation of stem cells to chondrogenic lineage whereas deviatoric or shear stress guides stem cells toward ligamentous and tendonous phenotypes [37]. In vitro studies have shown that such mechanical loading significantly affected terminally differentiated cells as well as lineage commitment in undifferentiated multipotent stem cells [8, 11, 14, 15, 22, 42, 43]. Specifically, shear forces by fluid flow have been shown to affect baseline gene expression of Collagen type I, II, Runx2 and Sox 9, which are markers of mesenchymal condensation [12, 34, 35, 37, 46] (Fig. 6).

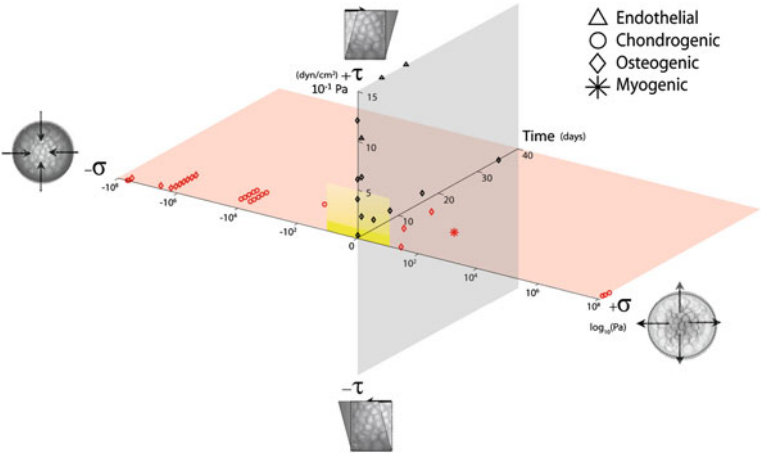

Fig. 5 Characteristic magnitudes and time domains of mechanical signals applied in studies of multipotent cell differentiation. *Red* data points dilatational stress and *black* data points deviatoric, i.e., shear stress. $-\sigma$ indicates hydrostatic compression and $+\sigma$ indicates tension depicted on a $\log_{10}$ scale in Pa. *Yellow* region shows dilatational and deviatoric stress ranges predicted to prevail during cell fate determination in utero. *Adapted from* [2, 41], used with permission

4 Stem Cell Morphology within Mechanical Environments

Stem cell shape has been shown to modulate fate or lineage commitment. Whereas flattened and spread shape directs stem cells toward osteogenesis, round and unspread shape directs stem cells toward adipogenesis. The RhoA-ROCK pathway, involving cytoskeletal remodeling of actin, has been shown to bridge stem cell shape changes to cell fate commitment [32].

The cytoskeleton is the main subcellular, mechanical support structure of the cell. Actin filaments and microtubules play a crucial role in the cellular response to external forces under fluid flow (Fig. 7). Recent studies show interesting relationships between stem cell shape and fate and the emergence of anisotropy in stem cells exposed to controlled dilatational and deviatoric stress environments. In these studies, larger cells at low cell density exhibit a more extensive cytoskeleton, as measured by amount of tubulin and actin expressed; in contrast, smaller cells at high cell density exhibit a less extensive cytoskeleton. Furthermore, expression of tubulin is more significantly affected by shear flow than expression of actin; this is particularly interesting, given tubulin's role in bearing compressive forces in the cell compared to actin, which withstands more tensile forces [12].

The role of nucleus shape change in fate determination is just beginning to be elucidated. A recent study demonstrated a significant relationship between nucleus shape and cell seeding protocol; namely, seeding at increasing target density changes the volume of the cell while changing the shape of the nucleus. Furthermore, changes in nucleus shape are significantly correlated to (fold) changes in

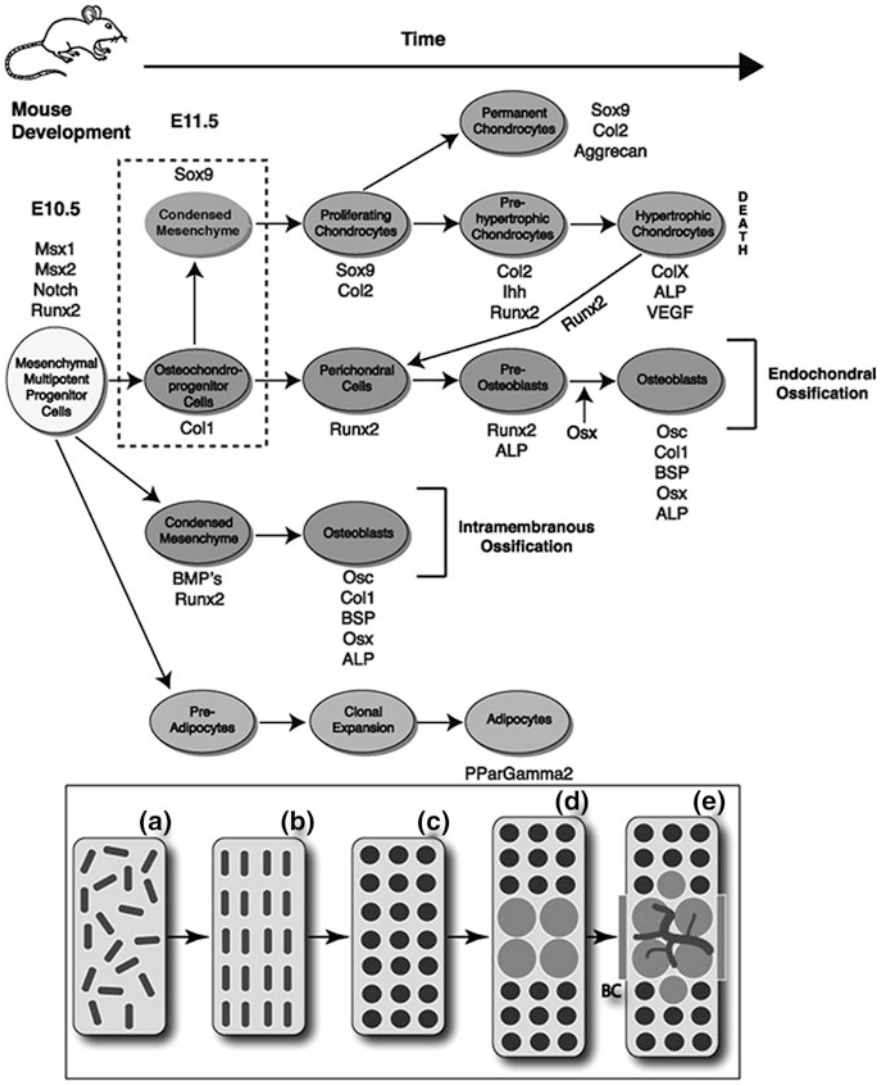

Fig. 6 Differentiation of mesenchymal stem cells into several lineages including chondrocytes (*orange* in online version of the figure), osteoblasts (*blue* in online version of the figure), and adipocytes (*green* in online version of the figure). (*Top*) Prior to mesenchymal condensation, upregulation of notch signals for chondrogenesis, which upregulates Sox9, one of the first transcription factors regulating endochondral ossification. (*Bottom*) In addition to direct formation of woven bone during intramembranous ossification (described in context of the one stage bone transport procedure), bone also forms via endochonral ossification, as shown schematically; cells (**a**) proliferate and organize into the condensed mesenchyme comprised of osteochondroprogenitor cells (**b**). The cells of the condensed mesenchyme differentiate into chondrocytes (**c**) and the cells at the center of the condensation stop proliferating and become hypertrophic (**d**). Perichondral cells adjacent to the hypertrophic chondrocytes differentiate into osteoblasts (**e**) and form the bone collar (**b**, **c**) as the invasion of blood vessels begins concomitant to continued osteoblast differentiation. *Adapted from* [27], used with permission. Please refer to online version of chapter for color version of the figure

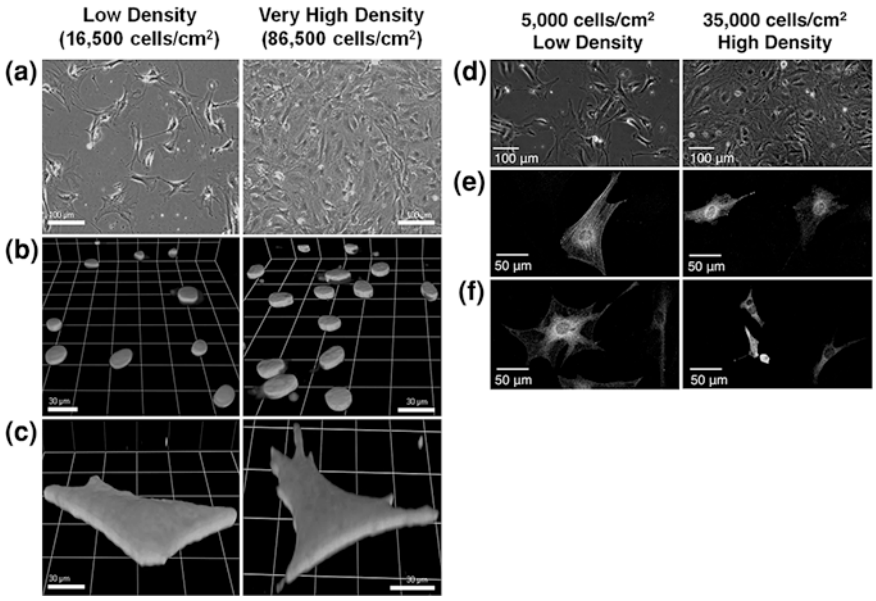

Fig. 7 Stem cell morphology changes at the subcellular length scale as a consequence of seeding at different densities and using different protocols to achieve density. **a**, **b**, **c** Nucleus shape changes **b** and cell shape changes **c** are attributable to target cell seeding densities and means of achieving density [12], used with permission. **d**, **e**, **f** The cytoskeleton components, including actin (**f**) and tubulin (**e**), also change when exposed to dilatational and deviatoric stress induced through different target densities and seeding protocols as well as exposure to fluid flow [46], used with permission. Please refer to online version of chapter for color version of the figure

gene expression of differentiation markers associated with mesenchymal condensation [46] (Fig. 7). Although correlation does not equal causation, it will be interesting to determine whether cell shape changes in response to mechanical signals are more of a response to minimize energy demands, e.g., by streamlining (laminar) flow to reduce losses associated with chaotic flow in boundary layers or as an active means for a cell to adapt to its environment (perhaps concomitant to reducing metabolic energy costs).

Computational methods can be applied to analyze cell deformations in near real time under shear flow; computational methods can predict deformation based on a given geometry and mechanical or chemical properties under external forces, which is passive behavior [7, 39]. On the other hand, active morphological changes of cells can occur through biological changes such as gene expression and reorientation of cytoskeletal filaments [10, 12, 31]. This active behavior can be also analyzed by computational models based on a given results under forces, which is an important approach to elucidate mechanisms of mechanoadaptation [17, 20, 31].

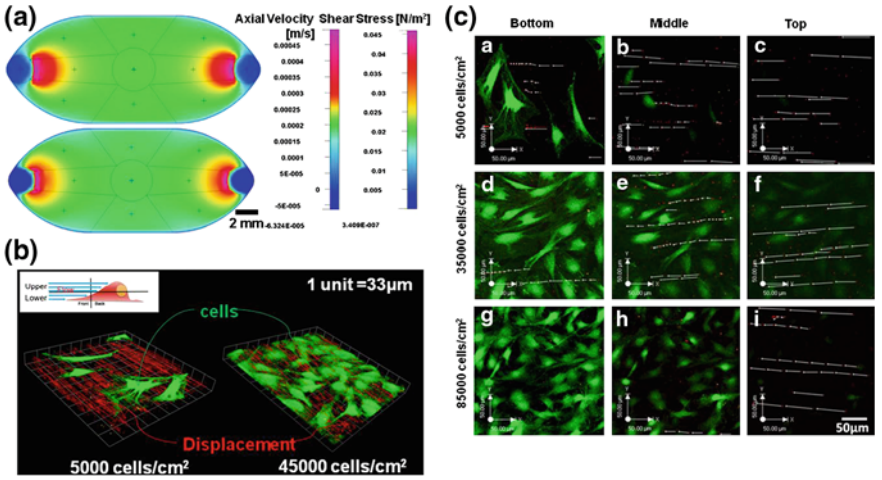

Fig. 8 CFD predictions and μ-PIV for flow regimes of interest. **a** CFD predictions of axial flow velocity (*upper*) and shear stress (*lower*) in the flow chamber at 10 μm from the bottom of the flow chamber. Flow moves from *right* (inlet) to *left* (outlet). **b** 3D images of flow fields (*red arrows* indicate microsphere displacements) around cells (*green*). Three dimensional confocal image stacks are analyzed to quantify the flow fields with respect to distance from the substrate and cell density. **d**– **l** Confocal images closest to the basal surface, approximately 2 μm from the substrate on which cells are seeded (**d**, **g**, **j**), 5 μm from the substrate (**e**, **h**, **k**), and 10 μm from the substrate (**f**, **i**, **l**). Cells are labeled with calcein *green*, microspheres exhibit *red fluorescence*, and white arrows indicated microsphere displacements in 990 ms. *Green*, *red*, and *white* indicate cells, microspheres, and displacements, respectively. *Adapted from* [40]

5 CFD Modeling for Precise Delivery of Mechanical Signals to MSCs to Direct Cell Fate

Based on CFD predictions, studies of parallel plate perfusion systems have underscored how important it is to translate signals delivered in two dimensions to three dimensions (3D), and at the subcellular length scale [1]. CFD can be used to predict flow regimes around cells (in 3D) in known flow chamber geometries and flow fields, to deliver controlled mechanical signals to cells seeded within. In situ microscopy allows for concomitant imaging of live cell mechano-adaptation while tracking the cell's dynamic mechanical environment [39, 41, 43]. Specifically, microscale particle image velocimetry (μ-PIV) allows not only for the validation of CFD predictions at the length scale of the coverslip (2D) and scaffolds (3D) onto which cells are seeded for mechanotransduction studies, but also for observing cell seeding effects on three dimensional flow field in the vicinity of cells. (Fig. 8, 9) Combined with rtPCR [34, 39, 41] and/or genetically modified stem cells that express green fluorescent protein upon differentiation.

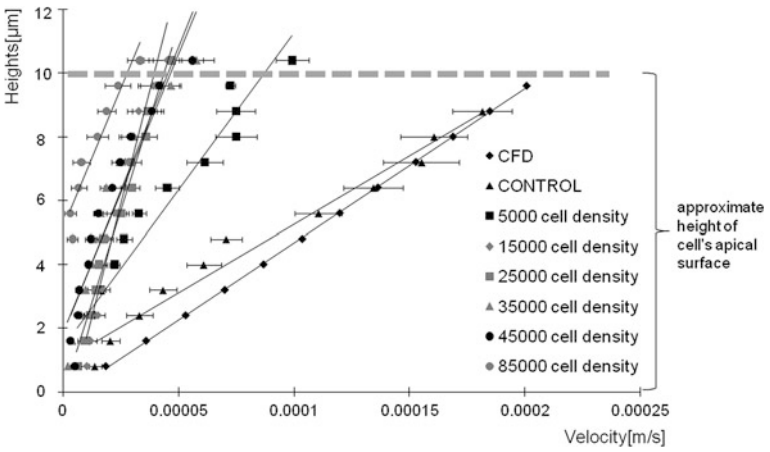

Fig. 9 CFD predictions compared to experimental measures (μ-PIV) of velocity in the flow chamber, in the absence of cells. Error bars report standard error (n = 5) at each data point. All linear regressions show $R^2 > 0.8$. The slopes of the linear regression lines represent the inverse of strain rate. *Adapted from* [40], used with permission

Flow is calculated from the continuity Eq. (1) and Navier–Stokes Eq. (2) using a second order upwind-discretization scheme in three dimensions. Wall shear stress is calculated from the wall strain rate (3). Hence,

$$\nabla \cdot v = 0, \tag{1}$$

$$\rho\ (v \cdot \nabla v)\Delta^2 v - \nabla P, \tag{2}$$

$$\tau_{cell} = \mu \frac{\partial v}{\partial x}\Big|_{cellheight}, \tag{3}$$

where v is the velocity vector, ρ is density, P is pressure, μ is viscosity, τ_{cell} is the shear stress at typical cell height, $\frac{\partial v}{\partial x}$ is the strain rate, and x is the height from bottom of chamber. (Fig. 8a).

CFD and microsphere displacement tracking enable the unprecedented prediction, validation and spatiotemporal delivery of mechanical signals on cell surfaces bordering other cells or the environment. This approach is rapidly translatable to the design of geometries and surfaces for tissue engineering scaffolds as delivery devices for mechanical and biochemical signals to steer the fate of cells seeded within.

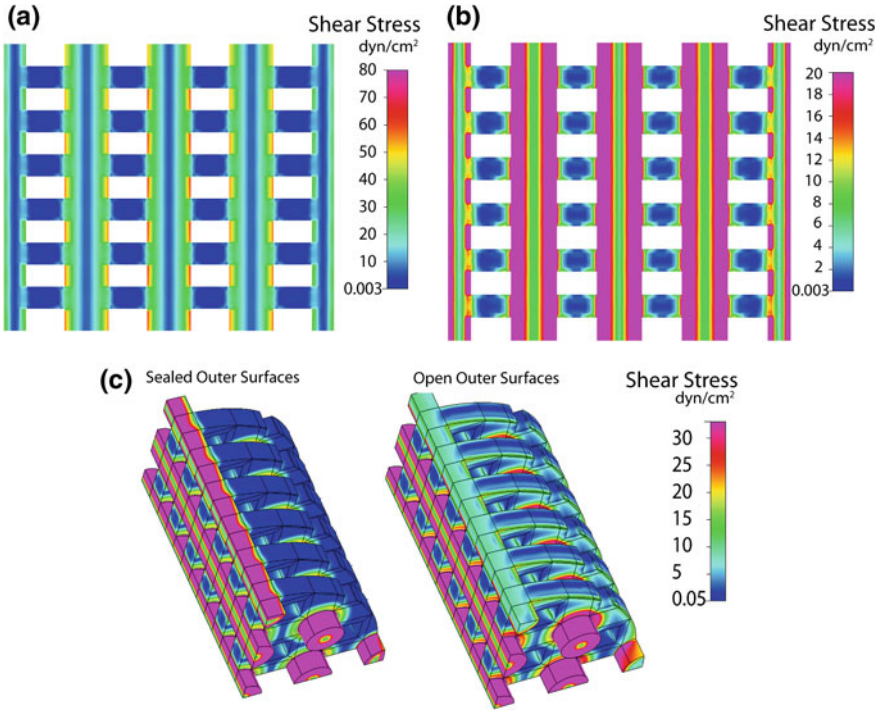

Fig. 10 CFD predicts shear stress to vary by an order of magnitude in longitudinal channels of a target tissue engineering scaffold geometry (80 dyn/cm^2, **a**, **c**) compared to transverse channels (10 dyn/cm^2, **b**, **c**). *Adapted from* [2], used with permission

6 CFD Modeling for Design of Tissue Engineering Scaffolds Geometry

Mechanically induced fluid movement through tissue engineering scaffolds provides a driving force for nutrient transport and waste removal. Furthermore, fluid flow can accelerate or activate bone development (osteogenesis and chondrogenesis) of MSCs [8, 11] through convective augmentation of anabolic biochemical factor transport or by delivery of mechanical cues at the interface between the fluid and the cell [2, 9, 23, 25].

A recently published CFD model explores effects of fluid flow in tissue engineering scaffolds designed to treat cranial defects (Fig. 2c). CFD predicts the different mechanical environments prevailing in longitudinal and transverse flow conduits, as well as on the conduit walls (inner surfaces of the scaffold) where cells are seeded (Fig. 10). Hence, by changing the size and relative geometry fluid channels in scaffolds, CFD can be used to optimize flow regimes within the scaffold to maintain nutrient and waste transport while achieving target mechanical stresses to guide stem cells toward target lineages using flow induced

Table 1 Effect of tissue engineering scaffold geometry (porosity and pore size) on fluid flow by CFD analysis

Reference	Scaffold type	Flow	Average shear surface rate (l/s) and stress (dyn/cm^2)
Anderson et al. [2]	Idealized design for critical sized critical defects Pore diameter: 800 μm Post diameter: 600 μm	Pressure gradient (Pa)	Longitudinal channels: 30–40 dyn/cm^2
		100	Transverseflow: 0–10 dyn/crn^2
Lesman et al. [30]	PLLA/PLGA scaffold Porosity: 90 % Average pore diameter: 500 μm	Inflow velocity (cm/s)	Four different cell layer thicknesses (0, 50, 75, 125 μm)
		0.5	2–18 dyn/cm^2
		1	
		1.5	
		2	
Voronov et al. [44]	Poly(L-Iacticacid) Porosity: 80–95% Average pore size: 215–402.5 μm	Pressure gradient (Pa)	
		10	~0.1 dyn/crn^2
		1	~0.01 dyn/cm^2
		0.1	~0.001 dyn/crn^2
		0.01	~0.0001 dyn/cm^2
Melchels et al. [36]	Photo-polymerisable poly(D/Llactide) (PDLLA) macromers Porosity: 62 ± 1 % Isotropic pore size: 412 ± 13 μm	Average fluid Flow velocity: 0.86 mm/s	15–24/s
	Porosity: 35–85 % Gradient in pore size: 250–500 μm		12–38/s
Y Yao et al. [45]	Idealized design with unit spherical cells porosity: 70 %	Flow rate: 0.l ml/min	0.03 dyn/cm^2
		Flow rate: 0.5 ml/min	0.15 dyn/cm^2
		Flow rate: 1 ml/min	0.3 dyn/cm^2

deviatoric stresses and seeding density and protocol induced dilatational stresses [2, 12, 34, 35, 38, 46].

CFD has also been used to optimize geometries of tissue engineered scaffolds that are manufactured using rapid prototyping or other methods. Furthermore, material choice will have a large effect on target and actual scaffold geometries and signal delivery [38]. Comparing two types of scaffolds, which are made by Collagen-Glycosaminoglycan (CG) and Calcium Phosphate, CFD predicts that shear stress is 2.8 times higher in the CG as in the calcium-phosphate scaffold. This is mainly caused by pore size differences (CG pore size ~96 mm, calcium phosphate pore size ~350 mm). A scaffold with bigger pore sizes (215–402.5 μm average pore size), made of Poly(L-lactic acid), has been also analysed using CFD

[21], which shows that different pore sizes and porosities cause different wall shear stress on surface of the scaffolds (Table 1) [2, 30, 36, 44, 45].

Flow regimes within a rapid prototyped scaffold have been studied previously to predict the effect of geometric discrepancies due to imperfect manufacturing, e.g., differences between target and actual manufactured scaffold geometries [38]. CFD can also be used to analyze differences in flow that are attributable to differences in actual geometries compared to target ideal geometries; for example, CFD accurately predicts the average fluid velocity across 81 % of the sample volume and the wall shear stress across 73 % of the sample surface, when compared to experimental validation of actual values using μ-PIV [16].

7 Conclusion

This chapter has outlined to major advantages of using CFD to design and optimize tissue engineering scaffold geometry, material behavior (including biodegradation), and tissue ingrowth over time. One major advantage is that CFD predicts flow conditions for precise delivery of mechanical signals to stem cells to direct cell fate (cell scale). A second advantage is that CFD can be used to optimize tissue engineering scaffold geometries, including pore size, pore distribution and connectivity, as well as scaffold wall thickness, to modulate flow regimes within the scaffold (tissue to cell scale). As multiscale CFD and finite element modeling approaches converge, we anticipate that multiscale modeling will become an even more powerful tool to predict cell-organ scale system behavior, seamlessly, over multiple time scales that span the life of the patient or test subject.

References

1. Anderson, E.J., Falls, T.D., Sorkin, A.M., Knothe Tate, M.L.: The imperative for controlled mechanical stresses in unraveling cellular mechanisms of mechanotransduction. Biomed Eng Online **5**, 27 (2006). doi:10.1186/1475-925X-5-27. 1475-925X-5-27 [pii]
2. Anderson, E.J., Knothe Tate, M.L.: Design of tissue engineering scaffolds as delivery devices for mechanical and mechanically modulated signals. Tissue Eng **13**, 2525–2538 (2007). doi:10.1089/ten.2006.0443
3. Anderson, E.J., Knothe Tate, M.L.: Design of tissue engineering scaffolds as delivery devices for mechanical and mechanically modulated signals. Tissue Eng **13**, 2525–2538 (2007). doi:10.1089/ten.2006.0443
4. Anderson, E.J., Knothe Tate, M.L.: Open access to novel dual flow chamber technology for in vitro cell mechanotransduction, toxicity and pharamacokinetic studies. Biomed Eng Online **6**, 46 (2007). doi:10.1186/1475-925X-6-46. 1475-925X-6-46 [pii]
5. Anderson, E.J., Kreuzer, S.M., Small, O., Knothe Tate, M.L.: Pairing computational and scaled physical models to determine permeability as a measure of cellular communication in micro- and nano-scale pericellular spaces. Microflu Nanoflu **4**, 193–204 (2008). doi:10.1007/s10404-007-0156-5
6. Anderson, E.J., Knothe Tate, M.L.: Idealization of pericellular fluid space geometry and dimension results in a profound underprediction of nano-microscale stresses imparted by fluid

drag on osteocytes. J Biomech **41**, 1736–1746 (2008). doi:10.1016/j.jbiomech.2008.02.035. S0021-9290(08)00107-3 [pii]
7. Bagchi, P., Johnson, P.C., Popel, A.S.: Computational fluid dynamic simulation of aggregation of deformable cells in a shear flow. J Biomech Eng **127**, 1070–1080 (2005)
8. Baksh, D., Tuan, R.S.: Canonical and non-canonical Wnts differentially affect the development potential of primary isolate of human bone marrow mesenchymal stem cells. J Cell Physiol **212**, 817–826 (2007). doi:10.1002/jcp.21080
9. Bonewald, L.F.: Mechanosensation and Transduction in Osteocytes. Bonekey Osteovision **3**, 7–15 (2006). doi:10.1138/20060233
10. Boon, R.A., Leyen, T.A., Fontijn, R.D., Fledderus, J.O., Baggen, J.M., Volger, O.L., van Nieuw Amerongen, G.P., Horrevoets, A.J.: KLF2-induced actin shear fibers control both alignment to flow and JNK signaling in vascular endothelium. Blood **115**, 2533–2542 (2010). doi:10.1182/blood-2009-06-228726. blood-2009-06-228726 [pii]
11. Campbell, J.J., Lee, D.A., Bader, D.L.: Dynamic compressive strain influences chondrogenic gene expression in human mesenchymal stem cells. Biorheology **43**, 455–470 (2006)
12. Chang, H., Knothe Tate, M.L.: Structure-function relationships in the stem cell's mechanical world B: emergent anisotropy of the cytoskeleton correlates to volume and shape changing stress exposure. Mol Cell Biomech **8**, 297–318 (2011)
13. Cooke MN, Fisher JP, Dean D, Rimnac C, Mikos AG (2003) Use of stereolithography to manufacture critical-sized 3D biodegradable scaffolds for bone ingrowth. J Biomed Mater Res B Appl Biomater 64: 65–69.doi:10.1002/jbm.b.10485
14. Datta, N., Pham, Q.P., Sharma, U., Sikavitsas, V.I., Jansen, J.A., Mikos, A.G.: In vitro generated extracellular matrix and fluid shear stress synergistically enhance 3D osteoblastic differentiation. Proc Natl Acad Sci USA **103**, 2488–2493 (2006). doi:10.1073/pnas.0505661103. 0505661103 [pii]
15. David, V., Martin, A., Lafage-Proust, M.H., Malaval, L., Peyroche, S., Jones, D.B., Vico, L., Guignandon, A.: Mechanical loading down-regulates peroxisome proliferator-activated receptor gamma in bone marrow stromal cells and favors osteoblastogenesis at the expense of adipogenesis. Endocrinology **148**, 2553–2562 (2007). doi:10.1210/en.2006-1704. en.2006-1704 [pii]
16. De, B.S., Truscello, S., Ozcan, S.E., Leroy, T., Van, O.H., Berckmans, D., Schrooten, J.: Bi-modular flow characterization in tissue engineering scaffolds using computational fluid dynamics and particle imaging velocimetry. Tissue Eng Part C Methods **16**, 1553–1564 (2010). doi:10.1089/ten.tec.2010.0107
17. Fletcher DA, Mullins RD (2010) Cell mechanics and the cytoskeleton. Nature **463**, 485–492. doi: 10.1038/nature08908, nature08908 [pii]
18. Gibson LJ, Ashby MF (1997) Cellular solids: structure and properties. In: Cambridge University Press, New York
19. Habal, M.B., Reddi, A.H.: Bone grafts and bone induction substitutes. Clin Plast Surg **21**, 525–542 (1994)
20. Inoue Y, Deji T, Shimada Y, Hojo M, Adachi T (2010) Simulations of dynamics of actin filaments by remodeling them in shear flows. Comput Biol Med 40: 876–882. doi: 10.1016/j.compbiomed.2010.09.008, S0010-4825(10)00137-X [pii]
21. Jungreuthmayer, C., Donahue, S.W., Jaasma, M.J., Al-Munajjed, A.A., Zanghellini, J., Kelly, D.J., O'Brien, F.J.: A comparative study of shear stresses in collagen-glycosaminoglycan and calcium phosphate scaffolds in bone tissue-engineering bioreactors. Tissue Eng Part A **15**, 1141–1149 (2009). doi:10.1089/ten.tea.2008.0204
22. Kearney, E.M., Farrell, E., Prendergast, P.J., Campbell, V.A.: Tensile strain as a regulator of mesenchymal stem cell osteogenesis. Ann Biomed Eng **38**, 1767–1779 (2010). doi:10.1007/s10439-010-9979-4
23. Knothe Tate ML (2003) Whither flows the fluid in bone? An osteocyte's perspective. J Biomech 36:1409–1424. S0021929003001234 [pii]
24. Knothe Tate ML (2007) Engineering of functional skeletal tissues, multiscale computational engineering of bones: state-of-the-art insights for the future, Springer, New York

25. Knothe Tate ML (2011) Top down and bottom up engineering of bone. J Biomech 44: 304–312. doi: 10.1016/j.jbiomech.2010.10.019, S0021-9290(10)00575-0 [pii]
26. Knothe Tate ML, Chang H, Moore SR, Knothe UR (2011) Surgical membranes as directional delivery devices to generate tissue: testing in an ovine critical sized defect model. PLoS One 6: e28702. doi: 10.1371/journal.pone.0028702, PONE-D-11-07884 [pii]
27. Knothe Tate ML, Falls TD, McBride SH, Atit R, Knothe UR (2008) Mechanical modulation of osteochondroprogenitor cell fate. Int J Biochem Cell Biol 40:2720–2738. doi: 10.1016/j.biocel.2008.05.011, S1357-2725(08)00198-2 [pii]
28. Knothe Tate ML, Ritzman TF, Schneider E, Knothe UR (2007) Testing of a new one-stage bone-transport surgical procedure exploiting the periosteum for the repair of long-bone defects. J Bone Joint Surg Am 89: 307–316. doi: 10.2106/JBJS.E.00512, 89/2/307 [pii]
29. Knothe UR, Dolejs S, Matthew MR, Knothe Tate ML (2010) Effects of mechanical loading patterns, bone graft, and proximity to periosteum on bone defect healing. J Biomech 43: 2728–2737. doi: 10.1016/j.jbiomech.2010.06.026, S0021-9290(10)00362-3 [pii]
30. Lesman, A., Blinder, Y., Levenberg, S.: Modeling of flow-induced shear stress applied on 3D cellular scaffolds: implications for vascular tissue engineering. Biotechnol Bioeng **105**, 645–654 (2010). doi:10.1002/bit.22555
31. Loufrani, L., Henrion, D.: Role of the cytoskeleton in flow (shear stress)-induced dilation and remodeling in resistance arteries. Med Biol Eng Comput **46**, 451–460 (2008). doi:10.1007/s11517-008-0306-2
32. McBeath R, Pirone DM, Nelson CM, Bhadriraju K, Chen CS (2004) Cell shape, cytoskeletal tension, and RhoA regulate stem cell lineage commitment. Dev Cell 6:483–495. S15345 80704000759 [pii]
33. McBride, S.H., Dolejs, S., Brianza, S., Knothe, U., Tate, M.L.: Net change in periosteal strain during stance shift loading after surgery correlates to rapid de novo bone generation in critically sized defects. Ann Biomed Eng **39**, 1570–1581 (2011). doi:10.1007/s10439-010-0242-9
34. McBride, S.H., Falls, T., Knothe Tate, M.L.: Modulation of stem cell shape and fate B: mechanical modulation of cell shape and gene expression. Tissue Eng Part A **14**, 1573–1580 (2008). doi:10.1089/ten.tea.2008.0113
35. McBride, S.H., Knothe Tate, M.L.: Modulation of stem cell shape and fate A: the role of density and seeding protocol on nucleus shape and gene expression. Tissue Eng Part A **14**, 1561–1572 (2008). doi:10.1089/ten.tea.2008.0112
36. Melchels FP, Tonnarelli B, Olivares AL, Martin I, Lacroix D, Feijen J, Wendt DJ, Grijpma DW (2011) The influence of the scaffold design on the distribution of adhering cells after perfusion cell seeding. Biomaterials **32**, 2878–2884. doi: 10.1016/j.biomaterials.2011.01.023, S0142-9612(11)00036-6 [pii]
37. Pauwels, F.: A new theory on the influence of mechanical stimuli on the differentiation of supporting tissue. The tenth contribution to the functional anatomy and causal morphology of the supporting structure. Z Anat Entwicklungsgesch **121**, 478–515 (1960)
38. Sanan, A., Haines, S.J.: Repairing holes in the head: a history of cranioplasty. Neurosurgery **40**, 588–603 (1997)
39. Song, M., Brady-Kalnay, S., Dean, D. Knothe Tate, M.L.: Relating Stem Cell Shape to Fate Commitment by Mapping Cell Surface Strains In Situ. Trans ORS **37**, 0826 (2012)
40. Song MJ, Dean D, Knothe Tate ML (2010) In situ spatiotemporal mapping of flow fields around seeded stem cells at the subcellular length scale. PLoS One 5. doi: 10.1371/journal.pone.0012796
41. Song, M.J., Dean, D., Brady-Kalnay, S., Knothe Tate, M.L.: Optimization of Tissue Engineering Scaffold Geometry, Seeding & Flow Conditions to Steer Stem Cell Shape and Fate. TERMIS 1, 0243 (2011)
42. Sorkin AM, Dee KC, Knothe Tate ML (2004) "Culture shock" from the bone cell's perspective: emulating physiological conditions for mechanobiological investigations. Am J Physiol Cell Physiol 287:C1527–C1536. doi: 10.1152/ajpcell.00059.2004, 00059.2004 [pii]
43. Stops AJ, Heraty KB, Browne M, O'Brien FJ, McHugh PE (2010) A prediction of cell differentiation and proliferation within a collagen-glycosaminoglycan scaffold subjected to

mechanical strain and perfusive fluid flow. J Biomech 43:618–626. doi: 10.1016/j.jbiomech.2009.10.037, S0021-9290(09)00624-1 [pii]
44. Voronov R, Vangordon S, Sikavitsas VI, Papavassiliou DV (2010) Computational modeling of flow-induced shear stresses within 3D salt-leached porous scaffolds imaged via micro-CT. J Biomech 43: 1279–1286. doi: 10.1016/j.jbiomech.2010.01.007, S0021-9290(10)00039-4 [pii]
45. YaoY, Chen W , Jin W: The influence of pore structure on internal flow field shear stress within scaffold. Adv Mater Res **308–310**, 771–775 (2011). doi:10.4028/www.scientific.net/AMR.308-310.771
46. Zimmermann JA, Knothe Tate ML (2011) Structure-function relationships in the stem cell's mechanical world A: seeding protocols as a means to control shape and fate of live stem cells. Mol Cell Biomech 8:275–296